Compressive Sensing of a Taylor-Fourier Multifrequency Model for Synchrophasor Estimation

Matteo Bertocco, *Member, IEEE*, Guglielmo Frigo, *Student Member, IEEE*, Claudio Narduzzi, *Member, IEEE*, Carlo Muscas, *Member, IEEE*, Paolo Attilio Pegoraro, *Member, IEEE*

***Abstract*—Synchrophasor measurements, performed by phasor measurement units (PMUs), are becoming increasingly important for power system network monitoring. Synchrophasor standards define test signals for verification of PMU compliance, and set acceptance limits in each test condition for two performance classes (P and M). Several PMU algorithms have been proposed to deal with steady-state and dynamic operating conditions identified by the standard. Research and discussion arising from design, implementation, testing and characterization of PMUs evidenced that some disturbances, such as interharmonic interfering signals, can seriously degrade synchrophasor measurement accuracy.**

In this paper, a new Compressive Sensing (CS) approach is introduced and applied to synchrophasor measurements using a Taylor-Fourier multifrequency model (CSTFM). The aim is to exploit, in a joint method, the properties of CS and the Taylor-Fourier transform to identify the most relevant components of the signal, even under dynamic conditions, and to model them in the estimation procedure, thus limiting the impact of harmonic and interhamonic interferences.

The CSTFM approach is verified using composite tests derived from the test conditions of the synchrophasor standard and simulation results are presented to show its potentialities.

***Keywords*—Phasor Measurement Units, Compressive Sensing, Taylor-Fourier Model, Synchrophasor, Orthogonal Matching Pursuit, IEEE C37.118.1**

I. Introduction

Phasor Measurement Units (PMUs) are the most innovative measurement devices in power network monitoring and are expected to become a fundamental tool for managing and supervising both transmission and distribution networks. IEEE Standard C37.118.1-2011 [1], along with its amendment [2], defines PMU outputs and applicable measurement accuracy limits. Synchrophasor, frequency and rate of change of frequency (ROCOF) measurements are introduced with the specific aim of describing the behavior of power network signals under dynamic conditions. Two performance classes are defined by the standard, M-class and P-class. The former is intended for measurement applications, where accuracy is emphasized, while the latter is designed for protection, which requires fast responses to dynamic events that can be critical for network operation.

Accuracy requirements are given for steady-state conditions, in the presence of off-nominal frequency, harmonic and interharmonic disturbances, as well as for dynamic conditions, considering amplitude and phase modulation, linear frequency ramp and step changes for both amplitude and phase-angle.

Several PMU algorithms have been proposed and characterized in the literature [3]–[16]. In [11] a demodulation and filtering approach, with frequency tuning, is followed to fulfill P- and M-class requirements, as suggested also by Annex C of [1]. Methods based on variable sampling period with phase-lock tracking, such as [7], [12], can be applied both to accurate synchrophasor estimation and to harmonic analysis.

In several works, slowly changing phasors are apporoximated with a complex Taylor series expansion around the estimation time point. In [4] and [5] synchrophasor estimation is enhanced by post-processing correction of estimation errors using sequential phasor estimates, computed with Discrete Fourier Transform (DFT) and Short-Time Fourier Transform (STFT). The Interpolated Discrete Fourier Transform (IpDFT) is used in [10], [16] to cope with static off-nominal conditions in synchrophasor and frequency estimation. In [14] the IpDFT is extended to compute the phasor derivatives of a second order expansion (thus, also frequency and ROCOF), from three DFT components around the fundamental frequency.

An algorithm based on a linear non-orthogonal transform, called the Taylor-Fourier filter (TFF) is introduced in [3] and in [6] a weighted least squares (WLS) approximation of an observation window is applied with respect to a second order Taylor model, providing a set of maximally flat Taylor-Fourier linear filters (WLS-TFF). In the following, these methods will be both generically referred to as Taylor weighted least squares (TWLS), for the sake of brevity, as in [13], because they differ in the specific weighting. TFF is generalized to harmonics as the Taylor-Fourier Transform (TFT) in [8].

A comparison of synchrophasor estimation performances under dynamic conditions was presented in [17] for some of the methods proposed in the literature. TWLS outperforms other methods reported in [17] in all dynamic conditions except under step tests, as confirmed in another set of comparative analyses [18]–[20]. An adaptive version of TWLS, which detects when the signal is undergoing fast changes and refines phasor estimation accordingly, was proposed in [21] and [22] to improve performance under transient conditions. A detection

M. Bertocco, G. Frigo and C. Narduzzi are with Department of Information Engineering of the University of Padova, Via Gradenigo 6/b, 35131 Padova, Italy (e-mail: [mat,frigogug,narduzzi]@dei.unipd.it).

C. Muscas, P. A. Pegoraro are with the Department of Electrical and Electronic Engineering of the University of Cagliari, Piazza d'Armi, 09123 Cagliari, Italy (email: [carlo, paolo.pegoraro]@diee.unica.it).

 DOI:10.1109/TIM.2015.2450295 Publisher version: http://ieeexplore.ieee.org/document/7164295/

approach, using the filtering paradigm, is used also in [23] to realize a hybrid M-class PMU with faster responses to transients and good measurement under steady state conditions.

Modifications and extensions of TWLS and TFT have been employed in PMU algorithm designs. In [24] frequency feedback is used to track the fundamental frequency and tune the TWLS filter accordingly. This adaptive algorithm is linked to a suitable detector to define a single output PMU [25] that complies with both P-class and M-class requirements for synchrophasor and frequency measurements, at the reporting rate of 50 frames/s. An efficient implementation of TFT filters is introduced in [26] and it is shown how frequency feedback can be used to redefine the center frequency of a TFT filter when the fundamental frequency is changing.

Great attention is being paid in providing estimation algorithms with the capability to cope with the kind of disturbances that can be found in the variable and quickly evolving scenarios of emerging power networks. A thorough discussion on the limits set by the synchrophasor standard and their physical meaning even saw the revision or suspension of some requirements [2].

Some disturbances, in particular those related to out-of-band (interharmonic) interfering signals, can be extremely difficult to deal with and can seriously affect synchrophasor, frequency and ROCOF estimation [23]. The presence of interharmonic components can have a very significant impact on the performance of a high-accuracy phasor estimator. In phasor analysis of harmonic signals, sampling is usually assumed to be quasi-synchronous with the power line frequency, so that spectral interference among signal components is limited. This allows the observation interval length to be a small number of cycles of the fundamental sine wave. However, the minimum distance between harmonic and interharmonic components can be far less than the separation between harmonics. As a consequence the effectiveness of windows, and Taylor-Fourier filters as well, in preventing the injection of out-of-band disturbances can be significantly impaired. Although filtering properties of longer observation intervals can be exploited [10], this reduces the ability to follow signal dynamics, as responsiveness to fast changing conditions asks for short observation windows and wider frequency pass-bands. In methods based on variable sampling frequency, rejection of interharmonic components also relies on effective filter design.

Very few assumptions can be made a priori with regards to interharmonics, which first raises the problem of their detection. In the extended Kalman filter implementation of [27] a DFT stage is employed to identify a single interfering out-of-band signal and filter it out by adding a notch to the Kalman model. If known, an interharmonic can be included in a Taylor-Fourier multifrequency model leading to perfect rejection of the disturbance [28].

Interharmonic detection requires the ability to scan frequencies with sufficient resolution, leading again, in principle, towards long observation intervals. However, recent research into the application of Compressive Sensing (CS) has shown that it is in fact possible to achieve frequency super-resolution or, alternatively, enhanced short-term performance [29], [30]. CS provides the opportunity to circumvent some limitations and estimate phasor components on a sufficiently fine frequency grid, while keeping the observation interval comparatively short even when interharmonics are involved [15].

The combined use of a CS approach for frequency support estimation and a TFT adapted to the CS stage outputs has been first investigated in [31] with a two-step estimation algorithm. In this paper, a unified compressive sensing Taylor-Fourier multifrequency (CSTFM) analysis is introduced, where frequency support estimation also considers higher-order derivatives, and allows simultaneous estimation of the phasor. The proposed approach is applied to synchrophasor measurement and tested under different conditions, with particular attention to out-of-band interference and possible concurrent disturbances.

II. Modeling for Accurate Phasor Measurement

A. Synchrophasor Dynamic Model

According to [1], the time-varying synchrophasor representation of a sinusoid signal $x(t)$, whose amplitude and frequency can vary with time, is given at the time instant t by:

$$\mathbf{X}(t) = \frac{X_m(t)}{\sqrt{2}} e^{j(2\pi \int g(t)\ dt + \phi_0)} \tag{1}$$

where ϕ_0 is the phase-angle at time $t_0 = 0$ and $g(t) = f(t) - f_0$ is the difference between the instantaneous frequency and the nominal power-line frequency f_0. With this notation the signal can be expressed as:

$$\begin{aligned} x(t) &= \mathrm{Re}\left[\sqrt{2}\mathbf{X}(t)e^{j2\pi f_0 t}\right] \\ &= \left[\frac{\mathbf{X}(t)}{\sqrt{2}} e^{j2\pi f_0 t} + \frac{\mathbf{X}^*(t)}{\sqrt{2}} e^{-j2\pi f_0 t}\right] \end{aligned} \tag{2}$$

The evolution of amplitude and phase-angle within the observation window, modeled in (1) by time-varying terms, can affect synchrophasor estimation.

The Taylor-Fourier approach [3] considers the Taylor expansion of the phasor $\mathbf{X}(t)$ around the reference time t_0, so that time variations occurring within the observation interval can be represented. It can be defined as the projection of signal $x(t)$ on a set of linearly independent basis functions:

$$\psi_k(t) = t^k e^{\pm j2\pi f_0 t}, \qquad k = 0,\ \ldots\ K. \tag{3}$$

When a finite sample record is considered, basis functions are replaced by their basis vector counterparts, $\psi_k[n]$. Legendre polynomials can also provide a basis for higher K but, in that case, derivatives would be computed indirectly [32].

Let $x[n]$ be a sequence of samples, having finite length N. In the following, N is assumed to be even and $-N/2 \leq n \leq N/2 - 1$, so that the time reference for the synchrophasor computation is located at $n = 0$ in the sample record. Using a K-th order expansion, the approximate model of the dynamic phasor becomes, in discrete form:

$$\mathbf{X}(nT) = \sum_{k=0}^{K} p^{(k)} \frac{(nT)^k}{k!} \tag{4}$$

where the complex number $p^{(k)}$ is the k-th order derivative of the dynamic phasor $\mathbf{X}(nT)$ at $n = 0$ and T is the sampling interval.

The Taylor-Fourier basis (3) is referred to the nominal frequency whereas, in practice, powerline fluctuations may occur. If the product ROCOF$\cdot NT/2$ is small enough in relation to f_0, the sinusoid frequency f_1 can be assumed to remain approximately constant within the observation interval, but may in general differ from the nominal value. A more accurate model could be obtained using f_1 in place of f_0 in (2) and (3). Thus, synchrophasor $\mathbf{X}_1(nT)$, where f_1 is taken as reference for the basis function, is considered instead of $\mathbf{X}(t)$, yielding:

$$x[n] = \mathrm{Re}\left[\sqrt{2}\mathbf{X}_1(nT)e^{j2\pi f_1 nT}\right] \tag{5}$$

Using the Taylor expansion, the signal can then be modelled as:

$$x[n] = \sum_{k=0}^{K} \frac{(nT)^k}{k!}\left[\frac{p_1^{(k)}}{\sqrt{2}}e^{j2\pi f_1 nT} + \frac{p_1^{*(k)}}{\sqrt{2}}e^{-j2\pi f_1 nT}\right] \tag{6}$$

where, as in (4), $p_1^{(k)}$ represents the k-th order derivative of the dynamic phasor $\mathbf{X}_1(nT)$ at $n = 0$.

B. Taylor-Fourier Multifrequency TFM Model

In actual conditions an electrical waveform can be represented as a multi-sine signal containing harmonics of the powerline frequency, as well as interharmonics. Its model is:

$$x[n] = \sum_h a_h[n]\cos(2\pi f_h nT + \phi_h[n]) \tag{7}$$

where a_h and ϕ_h are the (time-varying) amplitude and phase angle of the h-th component, respectively. For harmonics, f_h would be an integer multiple of f_1 (as, for instance, in [8]), otherwise it may represent a generic interharmonic frequency.

Defining a generic phasor:

$$\mathbf{X}_h[n] \triangleq \frac{a_h[n]}{\sqrt{2}}e^{j\phi_h[n]} \tag{8}$$

referred to frequency f_h, allows to extend the dynamic phasor approach to the generic signal (7), considering the Taylor expansion of each harmonic/interharmonic phasor $\mathbf{X}_h$. The signal can thus be approximated as:

$$x[n] = \sum_h \sum_{k=0}^{K_h} \frac{(nT)^k}{k!}\left[\frac{p_h^{(k)}}{\sqrt{2}}e^{j2\pi f_h nT} + \frac{p_h^{*(k)}}{\sqrt{2}}e^{-j2\pi f_h nT}\right] \tag{9}$$

where $p_h^{(0)}$ is the "average" harmonic/interharmonic phasor [17] and $p_h^{(k)}$ is the k-th derivative of the phasor at frequency f_h. For each component h a different order of expansion K_h may be used [9]. If frequencies f_h are known, the corresponding phasors can be computed from (9) along with their derivatives.

Model (9) provides the basis for analyses of different kinds, including the determination of harmonic phasors [8] and interharmonics. In the following it is referred to as TFM model, irrespective of the actual set of signal components covered by index h, but it should be emphasized that only a few relevant ones need to be explicitly considered for the purpose of synchrophasor estimation, such as interharmonics close to the fundamental frequency and, possibly, lower-order harmonics.

III. CSTFM Synchrophasor Estimation

A. Taylor-Fourier Basis and Sparsity

Let $\nu_h = f_h T$ be the signal component frequencies normalized by the sampling rate $1/T$. Given a sample record of size N, both DFT and Taylor-Fourier (TF) basis vectors refer to a set of N normalized frequencies $\nu_m = m/N$, with $m = 0, \ldots, N$. The corresponding set of N coefficients is defined on a uniform frequency grid with step $\Delta_f = 1/NT$.

Considering the same expansion order K for every h, (9) can be translated into matrix form as:

$$\mathbf{x} = \mathbf{B}\mathbf{p} + \mathbf{e} \tag{10}$$

where $\mathbf{x} = [x[-N/2], \ldots, x[+N/2-1]]^{\mathrm{T}}$ is the vector of signal samples. Columns of the $N \times (K+1)N$ matrix $\mathbf{B}$ are the TF basis vectors, defined by the discrete-time version of (3). Vector $\mathbf{p}$ has length $(K+1)N$ and is the concatenation of the N vectors $\mathbf{p}_h = \left[p_h^{(0)}, \ldots p_h^{(K)}\right]^{\mathrm{T}}$ for $h \in \{0, \ldots, N-1\}$:

$$\mathbf{p} = \left[\mathbf{p}_0^{\mathrm{T}}\ \mathbf{p}_1^{\mathrm{T}}\ \cdots\ \mathbf{p}_{N-1}^{\mathrm{T}}\right]^{\mathrm{T}}. \tag{11}$$

Finally, vector $\mathbf{e}$ represents noise, discrepancies between the mathematical model and experimental data, as well as any other contribution to uncertainty that may arise in the data acquisition system (e. g. because of analog-to-digital converter (ADC) quantization error).

In harmonic phasor analysis, elements $p_h^{(0)}$ differ from zero at frequency indexes h corresponding to the fundamental component and to harmonic terms. The same may be true of elements $p_h^{(k)}$ representing the dynamic extension of the phasor model. The condition $\|\mathbf{p}_h\|_2 \gg 0$, where $\|\cdot\|_2$ is the Euclidean norm of the vector, can therefore be associated with the presence of a non-negligible phasor component.

Since most vectors $\mathbf{p}_h$ will still be approximately zero, $\mathbf{p}$ can be considered a *sparse* or, more precisely, *block sparse* vector, which motivates interest in the formulation of (10) as a CS problem. However, if interharmonics are present the sparsity assumption is harder to meet.

B. Enhanced Resolution and Compressive Sensing

If a finer frequency grid with a smaller step $\Delta'_f = \Delta_f/P$ is considered, (with P a suitable integer), the total number of grid points becomes $N' = P \cdot N$ and signal component frequencies ν can be expressed as:

$$\nu_h = \frac{\hat{h} + \delta'_{\hat{h}}}{N'}, \qquad \text{with:} \quad |\delta'_{\hat{h}}| \le \frac{1}{2} \tag{12}$$

for some integer $\hat{h} \in [0, 1, \ldots, N'-1]$. The closest approximation to ν_h on the new grid is: $\hat{\nu}_{\hat{h}} = \hat{h}/N'$.

Defining a full set of TF basis vectors on this finer grid yields the generic basis vector expression:

$$\psi_k^h[n] = (nT)^k e^{j2\pi \frac{h}{N'} n}, \quad n = -N/2 \ \dots \ N/2-1 \quad (13)$$

where $h = 0, \dots, N'-1$ and the discrete normalized frequencies are now h/N'.

The creation of a finer frequency grid does not imply in itself a corresponding enhancement in the capability to resolve frequency components. To attain this or, equivalently, a shorter measurement interval with the same resolution, the use of an overcomplete dictionary to explicitly model the truncation effects related to finite observation length has been proposed in [29], [30].

From (9), using standard properties of Fourier transforms, one has the Fourier components:

$$X\left[\frac{m}{N}\right] = \sum_{h \in S_h} \left\{ \sum_{k=0}^{K} \frac{p_h^{(k)}}{\sqrt{2}} \left[\frac{1}{k!} \left(\frac{j}{2\pi} \right)^k D^{(k)} \left(\frac{m}{N} - \nu_h \right) \right] \right\}, \quad (14)$$

where $0 \le m < N$ and $D^{(k)}(\nu)$ is the k-th order derivative of the Dirichlet kernel:

$$D(\nu) = \frac{\sin \pi N \nu}{N \sin \pi \nu} \quad (15)$$

Replacing ν_h in (14) by its finite-grid approximation h/N' allows to reformulate the relationship in matrix form with Taylor-Fourier coefficients defined on the finer frequency grid. In the time domain the resulting equation is:

$$\mathbf{x} = \mathbf{W}^H \sum_{k=0}^{K} \mathbf{D}^{(k)} \mathbf{p}^{(k)} \quad (16)$$

where $\mathbf{p}^{(k)} = \left[p_0^{(k)} \ p_1^{(k)} \ \dots \ p_{N'-1}^{(k)} \right]^T$ and $[\mathbf{D}^{(k)}]_{m,h} = D^{(k)}(\frac{m}{N} - \frac{h}{N'})$. The columns of matrix $\mathbf{W}^H$ are the vectors of the DFT basis set. The superscript denotes conjugate transposition and it should be reminded that $\frac{1}{N}\mathbf{W}$ defines the DFT operation in matrix form.

By suitably recombining matrices and vectors, (16) can be rewritten in a form equivalent to (10):

$$\mathbf{x} = \mathbf{W}^H \mathbf{D} \mathbf{p} + \mathbf{e} \quad (17)$$

where $\mathbf{p}$ is still obtained by concatenation, as in (11), but here its length has grown to $(K+1)N'$. It should be noticed that the size of $\mathbf{W}^H$ is $N \times N$, while $\mathbf{D}$ has size $N \times (K+1)N'$. The latter is an overcomplete dictionary which explicitly models spectral leakage and accounts for both Taylor expansion and sparsification. Accordingly, CSTFM analysis is formulated as a CS problem, whose solution is:

$$\hat{\mathbf{p}} = \arg\min_{\mathbf{p}} \|\mathbf{p}\|_0 \quad \text{subject to: } \|\mathbf{x} - \mathbf{W}^H \mathbf{D} \mathbf{p}\|_2 \le \zeta \ , \quad (18)$$

where the pseudo-norm $\|\mathbf{p}\|_0$ indicates the number of non-zero elements of $\mathbf{p}$ and ζ is a given threshold.

Dictionary-based relationships (16), (17) imply a significant difference from other approaches, in the way the adverse effects on accuracy of a finite observation length are dealt with. In the proposed algorithm, spectral effects of truncation are explicitly modelled by matrix $\mathbf{D}$, that is defined over the finer frequency grid. It has to be emphasized that it is the presence of $\mathbf{D}$ that makes the block sparsity assumption for $\mathbf{p}$ hold approximately even when interharmonics are present.

This allows to position the Taylor-Fourier filters center frequencies much closer to actual component frequencies. At the same time, if two signal components are close, solving (18) disentangles reciprocal contributions even when some degree of interference occurs. This preserves accuracy, while the minimum observation interval length can remain shorter.

C. CSTFM Algorithm

Solution (18) can be found by a greedy algorithm, such as Orthogonal Matching Pursuit (OMP) [33]. The block-sparse feature of $\mathbf{p}$ can be exploited to speed-up the process.

The algorithm is iterative, starting from the given measurement vector $\mathbf{x}$ defined above. Let $\hat{\mathbf{p}}(i)$ be the vector estimate at the i-th iteration and $\hat{\mathbf{x}}_i = \mathbf{W}^H \mathbf{D} \hat{\mathbf{p}}(i)$ the corresponding signal reconstruction, where it is assumed $\hat{\mathbf{x}}_0 = \mathbf{0}$. At each iteration the index $\hat{h}_i$ of the largest frequency component, approximated to the nearest bin in the N'-point grid, is found as:

$$\hat{h}_i = \arg \max_{0 \le h < N'} \|(\mathbf{D}^{(0)})^{\mathrm{H}} \tfrac{1}{N} \mathbf{W} (\mathbf{x} - \hat{\mathbf{x}}_{i-1})\|_2, \quad (19)$$

and is included in the set: $\hat{S}_h(i) = \{\hat{h}_1, \dots, \hat{h}_i\}$ providing the frequency estimates (indexes of image components need to be checked as well). The set $\hat{S}_h(i)$ is called the *support* of vector $\hat{\mathbf{p}}(i)$ at iteration i. Support cardinality is equal to the iteration number, i.e., $|\hat{S}_h(i)| = i$.

For this step of the algorithm, only the zero order matrix $\mathbf{D}^{(0)}$ is involved. Here block sparsity comes into play since, once the index of a static phasor component has been located, the corresponding indexes for matrices $\mathbf{D}^{(1)}$ and $\mathbf{D}^{(2)}$ are easily determined.

Next, a reduced matrix of dictionary elements $\mathbf{D}_{\hat{S}_h(i)}$ is obtained by keeping only the columns of the full matrix $\mathbf{D}$ whose indexes belong (or are related) to $\hat{S}_h(i)$. Model coefficient estimates are computed by solving the reduced system:

$$\mathbf{x} = \mathbf{W}^H \mathbf{D}_{\hat{S}_h(i)} \hat{\mathbf{p}}(i) \quad (20)$$

The current solution $\hat{\mathbf{p}}(i)$ is updated and the corresponding signal reconstruction $\hat{\mathbf{x}}_i = \mathbf{W}^H \mathbf{D} \hat{\mathbf{p}}(i)$ is computed. This will be subtracted from the measurement vector $\mathbf{x}$ to compute the residue at the next iteration.

Suitable termination criteria, or a combination of them, must be defined. Typically, either the current residual norm is lower than threshold ζ in (18), or the maximum iteration number (maximum assumed support cardinality) has been reached.

The CS approach requires a minimum frequency separation of approximately $1.5 \cdot \Delta_f$ between two equal-magnitude waveform components lying on the fine grid [30]. When this condition is satisfied, the indices h can be determined correctly to within $\pm(\Delta_f/2P)$, that is, with the enhanced resolution provided by the finer grid. It should be remembered this value cannot be made arbitrarily small, as the numerical conditioning of $\mathbf{D}$ tends to get worse for large P. Improvement by about one order of magnitude is, however, achievable.

D. Computational considerations

The OMP algorithm consists in the iterative execution of two main stages: enhanced-resolution identification of the signal spectral support and TFM-based phasor estimation. The contribution to overall computational cost of each OMP iteration step can be assessed in terms of basic arithmetic operations as follows:

- as a first iteration step, the current residue vector $\mathbf{x} - \hat{\mathbf{x}}_{i-1}$ is multiplied by $(\mathbf{D}^{(0)})^H \frac{1}{N}\mathbf{W}$. This would require a total of $N' \cdot N$ multiplications and $N' \cdot (N-1)$ additions, but the same result is obtained more efficiently by zero-padding the residue to length $N' = NP$ and computing the DFT. Hence, the total number of operations is actually O($N(\log N + 2P - 1)$)
- support recovery (19) requires a search for the maximum, whose complexity is proportional to the size of vector $\mathbf{p}$. Hermitian symmetry allows to limit the search range to $0 \leq h < N'/2$ and this can be further restricted. In particular, the first OMP iteration aims to locate the index of the fundamental frequency. If the observation interval is about W cycles, this will fall in the neighborhood of $h = WP$ and the search range can be limited accordingly. In subsequent iterations, the search can in most cases be restricted to an approximate range $0 \leq h \leq k \cdot WP$, with $k \geq 2$. Since $W \ll N$, computational burden is significantly reduced;
- once the updated support $\hat{S}_h(i)$ has been determined, a pseudo-inverse solution to (20) has to be calculated. Its expression is:

$$\hat{\mathbf{p}}(i) = \left[\mathbf{D}^H_{\hat{S}_h(i)}\mathbf{D}_{\hat{S}_h(i)}\right]^{-1}\mathbf{D}^H_{\hat{S}_h(i)}\mathbf{W}\mathbf{x} \qquad (21)$$

  and it should be remarked that only the reduced matrix $\mathbf{D}_{\hat{S}_h(i)}$, composed of just $(K+1)\cdot i$ columns, is involved. Computation of the inverse requires O($[(K+1)\cdot i]^3$) operations and the overall computation of the pseudoinverse solution requires a further O($N \cdot [(K+1)\cdot i]^2$) operations. It is assumed that matrix $\mathbf{D}$ is pre-computed and stored in a dedicated memory area. Although this may be somewhat expensive in terms of storage, it allows to avoid the generation of a TF basis element at each iteration;
- finally, the new signal reconstruction is calculated and the current residual obtained by simple vector subtraction, corresponding to O($N \cdot [(K+1)\cdot i]$) operations.

Comparing CSTFM with other approaches, it is clear that greater computational costs are incurred as a result of the built-in adaptiveness. Additional effort is required to locate the fundamental frequency on a finer grid and, more importantly, iterations are carried out to discover and locate potential interferers that would impair measurement accuracy. Nevertheless, complexity of each iteration is little more than linear in the number of samples N.

One of the keys to algorithm sustainability is the choice of a suitably simple TFM model, so that cardinality of the support of $\mathbf{p}$ is kept low and, consequently, fewer iterations are required. Of course, total computational cost increases with the number of components modeled by (9), but so does measurement accuracy. The process can be made adaptive, if needed, by using an OMP termination criterion based on the threshold ζ, rather than a pre-determined model order.

Computation requirements are not beyond the possibilities of a well-designed implementation, and it can be noted that steps discussed above would all benefit significantly from parallelized implementation on a field-programmable gate array (FPGA). Even on a standard processor the number of OMP iterations can be managed since, as a consequence of the sparsity assumption and the use of a reduced TFM model, support cardinality (that is, the column dimension of submatrix $\mathbf{D}_{\hat{S}_h(i)}$) is limited and expected not to exceed $i_{MAX} \ll 10$.

Any practical implementation would have to provide a tradeoff between synchrophasor measurement accuracy and reporting rate.

IV. Tests and Results

In this section evaluation of the proposed algorithm performance under different conditions is discussed and results reported. Test signals for both M and P class PMUs, inspired by those indicated in [1] for individual operating conditions at the maximum reporting rate of 50 frames per second (fps), are mixed to create test signals representative of harder conditions in a changing environment.

Several configurations have been reproduced in the MatLab programming environment. Specifically, in each test condition the additional presence of interharmonics is considered. Care is taken to ensure that spurious components do not fall on any pre-determined point of the frequency grid and do not exhibit any degree of regularity. Frequency separation between the fundamental and the nearest interharmonic is assumed to be at least equal to half the reporting rate [1]. Additive white noise at a signal-to-noise ratio (SNR) of 60 dB is always superimposed on test signals to reproduce the effect of uncertainty and, in particular, sample quantization. A constant sampling rate is assumed, equal to 5000 samples/s. in nominal conditions, powerline frequency is $f_0 = 50$ Hz and the CS interpolation factor is $P = 10$.

Total vector error (TVE), which measures the relative deviation between the theoretical phasor and the estimated one, is the main accuracy index in the following. Results are provided in terms of TVE average value and standard deviation.

In a preliminary test, an interharmonic disturbance at $f_{ih} = 76$ Hz, whose amplitude is $10\,\%$ of that of the fundamental, has been added to a sinusoidal signal at the nominal frequency. Although frequency separation is slightly greater than the specified minimum, with respect to the TFM frequency grid defined by the parameters given above, interharmonic location is in fact as close as possible to worst-case for the CSTFM algorithm.

Table I compares results obtained for a single sinusoid plus noise (first two columns) with those obtained for the test signal (second two columns) and shows the impact of window length on 50 Hz phasor TVE. Four window lengths, corresponding to 2, 3, 5 and 7 nominal cycles, are used.

An observation interval of at least three cycles is required to deal with the interharmonic component. This is also the

TABLE I. CSTFM TOTAL VECTOR ERROR VS WINDOW LENGTH
SNR = 60 dB – WITHOUT/WITH INTERHARMONIC

	$f_1 = 50$		$f_1 = 50, f_{ih} = 76$	
Window length [nominal cycles]	**Avg TVE [%]**	**Std TVE [%]**	**Avg TVE [%]**	**Std TVE [%]**
2	0.022	0.012	–	–
3	0.013	0.006	0.088	0.121
5	0.010	0.005	0.011	0.005
7	0.008	0.004	0.008	0.005

minimum separation at which spectral interference can be considered negligible (in this case, $1.5 \cdot \Delta_f = 25$ Hz), although the interharmonic localization is still slightly affected, on account of its smaller magnitude and of the fact that the component has purposely been located off-grid. The resulting inaccuracy causes TVE to be larger than in the no-interharmonic case. It is also clear that longer observation intervals give lower TVEs, because of the enhanced frequency resolution and narrower bandwidth, which also improve noise rejection.

In all the tests that follow, the observation interval will be five nominal powerline cycles long, with $N = 500$ samples. Accordingly, frequencies can be determined to within less than ± 0.5 Hz and for the CSTFM algorithm interference among spectral components is negligible up to a minimum frequency separation of 15 Hz. In the static conditions of Table I, this ensures that the effect of the interharmonic on the TVE is negligible.

A. *Tests under steady state conditions*

Exhaustive comparison among all synchrophasor algorithms is beyond the scope of this paper. In the discussion that follows, results from three algorithms are considered:

- the classical TFF provided the basis for development of CSTFM. For this reason, it is selected to provide baseline results;
- in frequency-tracking algorithms, a harmonic model is matched to the signal under analysis, improving accuracy when the fundamental frequency is off-nominal and/or slowly varying. In this work, the CS frequency estimate of the first component found was employed to implement a TFF filter with adjustable center frequency, similarly to [24] but without interharmonic rejection. This algorithm is indicated as f-TFF;
- the third and final algorithm is CSTFM.

Table II reports TVE obtained, in a 2-s test with the same signals considered above, for TFF, f-TFF and the proposed CSTFM method. When only the 50 Hz component is present, the three methods yield the same performance, which is not surprising, as all stem from the basic Taylor-Fourier approach. The TFM model allows rejection of interharmonic interference and shows the best estimation performance in that case. Although the fundamental frequency component is always correctly identified, neither TFF nor f-TFF are designed to explicitly account for the interharmonic component and their accuracy suffers accordingly.

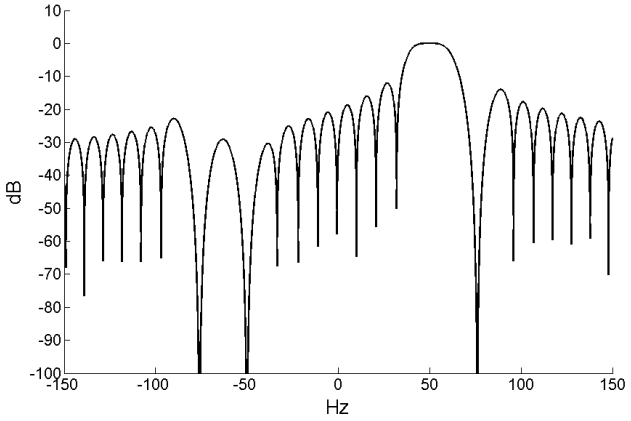

Fig. 1. Example of instantaneous frequency response of CSTFM in the presence of an interharmonic at 76 Hz, with $K = 2$ for each component.

The frequency response of the CSTFM synchrophasor estimation filter for the test condition of Table II, at a specific reporting instant, is plotted in Fig. 1. It clearly shows how the inclusion of the estimated interharmonic frequency in the model adds a zero (the multiplicity depends on the order of the Taylor expansion) at such frequency.

Fig. 2 reports results of the out-of-band tests for the two limiting off-nominal frequencies given by the standard at 50 fps ($f_1 = 47.5$ Hz and $f_1 = 52.5$ Hz) when the out-

TABLE II. TOTAL VECTOR ERROR ALGORITHM COMPARISON
SNR = 60 dB – WITHOUT/WITH INTERHARMONIC

	$f_1 = 50$ Hz, no interharmonic		$f_1 = 50$ Hz, $f_{ih} = 76$ Hz	
Method	**Avg TVE [%]**	**Std TVE [%]**	**Avg TVE [%]**	**Std TVE [%]**
TFF	0.010	0.005	1.305	0.147
f-TFF	0.010	0.005	1.305	0.147
CSTFM	**0.010**	**0.005**	**0.011**	**0.005**

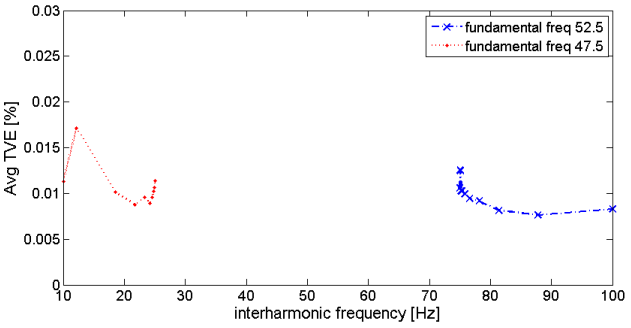

Fig. 2. TVE mask with different out-of-band interfering frequency and off-nominal frequency. Interharmonic amplitude is 10 % of the fundamental.

of-band frequency varies in the ranges $[10\,\text{Hz}, 25\,\text{Hz}]$ and $[75\,\text{Hz}, 100\,\text{Hz}]$. Interharmonics, of the same level as in previous tests, are selected according to IEEE C37.242 guide for PMU testing [34], noise level is the same as in previous tests. It can be observed that TVE behaviour is quite flat, because, if correctly identified, interfering frequencies are filtered out in each case.

In the next test, a $10\,\%$ second or third order harmonic ($f_h = 100$ Hz or $f_h = 150$ Hz, respectively) is superimposed on a sinusoid at nominal frequency 50 Hz, in addition to the interharmonic signal at $f_{ih} = 76$ Hz. Table III reports results for f-TFF and CSTFM with a three-component TFM model. TFF results were identical to those of f-TFF, as in Table II, so they are not reported. While benefits of CSTFM are clear, it can also be noticed that TVE for f-TFF in the third harmonic case is nearly the same of Table II. This suggests that, at that distance from the fundamental, attenuation introduced by synchrophasor estimation filters is large enough.

TABLE III. TOTAL VECTOR ERROR ALGORITHM COMPARISON
SNR = 60 dB – INTERHARMONIC PLUS 2ND/3RD HARMONIC

	$f_h = 100$ Hz, $f_{ih} = 76$ Hz		$f_h = 150$ Hz, $f_{ih} = 76$ Hz	
Method	**Avg TVE [%]**	**Std TVE [%]**	**Avg TVE [%]**	**Std TVE [%]**
f-TFF	1.325	0.260	1.307	0.158
CSTFM	**0.011**	**0.006**	**0.011**	**0.005**

To verify the effectiveness of a reduced-order TFM model, a test signal including harmonics up to 5-th order with decreasing magnitudes (respectively, 6.5%, 2.5%, 1% and 0.5% of the fundamental component), together with a 76-Hz interharmonic and 60-dB SNR was considered. Total root-mean-square (rms) harmonic and interharmonic distortion is 12% of the fundamental rms value.

The CSTFM algorithm was applied considering first a single phasor (fundamental only), then a two-phasor (fundamental plus interharmonic), a three-phasor and, finally, a four-phasor model (fundamental, interharmonic second and third harmonic). In the latter case rms distortion due to unmodelled components is just 1.1% of the fundamental rms value, but still affects TVE to some extent. As shown in Table IV, modelling three components at least is essential in this case.

In the final set of static tests a severely off-nominal sinusoidal signal at either 45 Hz or 55 Hz (maximum deviations for M-class PMU off-nominal frequency tests [1]) is combined with a single interharmonic interfering signal at either

TABLE IV. TVE FOR REDUCED-ORDER TFM MODEL
SNR = 60 dB – INTERHARMONIC PLUS HARMONICS UP TO 5TH ORDER

Modelled phasors	**Avg TVE [%]**	**Std TVE [%]**
f_1	1.315	0.203
f_1 and f_{ih}	0.749	0.221
f_1, $2f_1$ and f_{ih}	0.272	0.075
f_1, $2f_1$ $3f_1$ and f_{ih}	0.072	0.021

TABLE V. TVE FOR OFF-NOMINAL FUNDAMENTAL FREQUENCY
SNR = 60 dB – INTERHARMONIC

Test	**Method**	**Avg TVE [%]**	**Std TVE [%]**
$f_1 = 45$ Hz, $f_{ih} = 21.5$ Hz	*TFF*	2.101	0.771
	f-TFF	2.377	0.530
	CSTFM	**0.013**	**0.007**
$f_1 = 55$ Hz, $f_{ih} = 21.5$ Hz	*TFF*	2.092	0.632
	f-TFF	1.593	0.417
	CSTFM	**0.010**	**0.005**
$f_1 = 45$ Hz, $f_{ih} = 76$ Hz	*TFF*	2.331	1.106
	f-TFF	1.184	0.196
	CSTFM	**0.011**	**0.005**
$f_1 = 55$ Hz, $f_{ih} = 76$ Hz	*TFF*	2.341	0.950
	f-TFF	2.252	0.197
	CSTFM	**0.013**	**0.006**

$f_{ih} = 76$ Hz or $f_{ih} = 21.5$ Hz with amplitude $10\,\%$ of the fundamental component. Of the selected interharmonic frequencies, both in the out-of-band frequency region suggested by [1], the former is off the standard N-point frequency grid, the latter lies even off the finer grid.

Table V compares test outcomes for the same three algorithms of Table II. Strong interference from the interharmonic is the dominant issue and, as already noted, neither f-TFF nor TFF are designed to deal with it. However, it can be noticed that, for the test frequencies given in the first row of Table V, TFF outperforms f-TFF. In this case, tuning the f-TFF filter at the correct frequency brings it closer to the interharmonic and actually reduces attenuation of the out-of-band component. This emphasizes the importance of including the identified interharmonic in the TFM model.

The super-resolution afforded by the CSTFM approach allows frequency tuning also for the interharmonic, that leads to TVE under off-nominal conditions being comparable to that at nominal frequency.

Another important issue in out-of-band tests is frequency error (FE), for which stringent requirements are set in [1]. As an example, the values reported in Table VI refer to CSTFM algorithm performance in the test conditions of Tables III and V. The results only consider a direct frequency estimation obtained by means of the phasor first derivative.

B. Tests under dynamic conditions

According to IEEE Standard C37.118.1a-2014 [2], synchrophasor measurement bandwidth is determined by tests with amplitude modulation (AM) and phase modulation (PM) of the sinusoidal signal at nominal frequency. Two modulated signals are adopted for the tests, keeping the same configuration of noise and interharmonic disturbances:

- AM with modulation level $k_x = 0.1$ and modulation frequency $f_m = 5$ Hz;

TABLE VI. CSTFM FREQUENCY ERRORS – SNR = 60 dB

	Test conditions					
f_1 [Hz]	45	55	45	55	50	50
f_{ih} [Hz]	21.5	21.5	76	76	76	76
f_h [Hz]	-	-	-	-	100	150
Avg FE [mHz]	0.36	0.20	0.28	0.25	0.26	0.26
Std FE [mHz]	0.29	0.16	0.19	0.19	0.17	0.17

TABLE VII. TVE WITH AMPLITUDE AND PHASE MODULATIONS SNR = 60 dB – INTERHARMONIC

Test	Method	Avg TVE [%]	Std TVE [%]
AM $k_x = 0.1$, $f_m = 5$ Hz,	*f-TFF*	1.326	0.208
$f_{ih} = 76$ Hz	***CSTFM***	0.119	0.046
PM $k_a = 0.1$, $f_m = 5$ Hz,	*f-TFF*	1.299	0.273
$f_{ih} = 76$ Hz	***CSTFM***	0.124	0.039

- PM with modulation level $k_a = 0.1$ and modulation frequency $f_m = 5$ Hz (corresponding to the maximum values indicated by [2] for M-class).

Table VII shows TVE results for both f-TFF and the proposed method. It is clear that rejection of the interharmonic, by its estimation and inclusion in the model, leads to lower measurement errors also under dynamic conditions. Residual error is higher than in Table II, due to the passband of the estimation filters affecting the modulated signals.

CSTFM algorithm performance has been characterized also during a linear ramp of the fundamental frequency. The ramp ROCOF has been set to 1 Hz/s, as indicated by the standard, and a 10-s test has been performed, thus letting the frequency change in the range $[45, 55]$ Hz.

Fig. 3 shows a plot of percent TVE when noise and a 76-Hz interhamonic are present during the whole ramp duration. With CSTFM an average TVE of about $0.01\,\%$ (with a standard deviation of $0.016\,\%$) is reached during the ramp and similar results can be obtained changing the interharmonic frequency. To help evidence the CSTFM trace, the inset box shows the first half of the full plot with a logarithmic vertical scale.

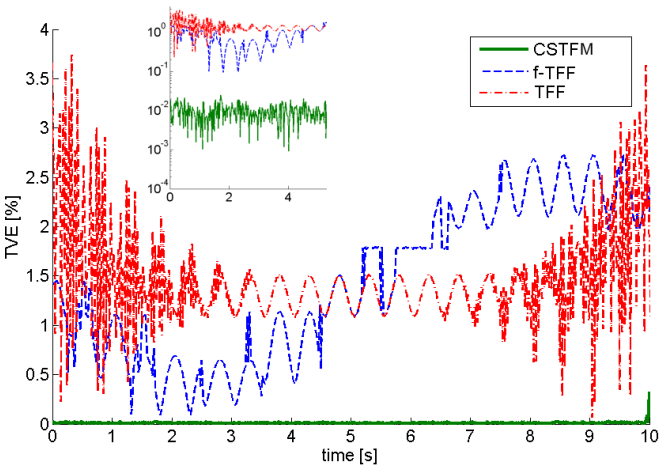

Fig. 3. TVE trends during ramp frequency test (with interharmonic and noise). In the zoomed inset box a logscale vertical axis is used.

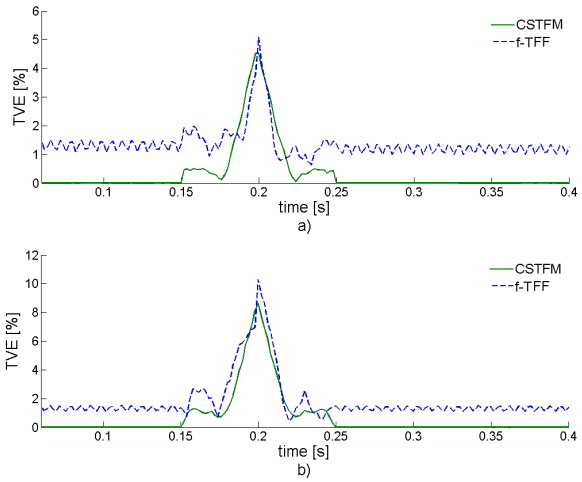

Fig. 4. TVE trends in the presence of step changes (with interharmonic and noise): a) $+10\,\%$ amplitude step; b) $+10°$ phase-angle step.

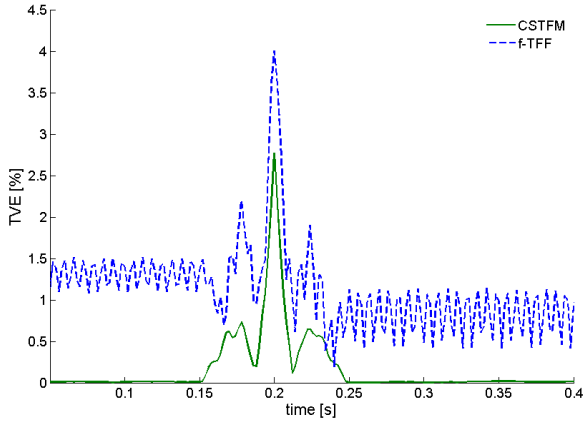

Fig. 5. TVE in the presence of a frequency step change from 50 Hz to 49 Hz.

Tracking of the fundamental frequency by f-TFF yields better results in the first part of the ramp. As the fundamental shifts towards higher frequencies, getting closer to the interharmonic, the same phenomenon mentioned above occurs and TFF actually outperforms it.

The step response of the CSTFM algorithm has been verified with both amplitude ($\pm 10\,\%$) and phase-angle ($\pm 10°$) steps applied to a sinusoidal signal at nominal frequency [1]. Plots in Fig. 4 show that algorithm response time, defined as the time required to bring TVE back to $\leq 1\%$, is about 32 ms for amplitude and 88 ms for phase-angle steps, respectively. The parameter cannot be defined for f-TFF, as TVE is always larger than $1\,\%$ even in the pre- and post-step steady-state conditions. Delay time of CSTFM in such tests is < 0.4 ms, because of

the practically centered reference time and symmetric nature of the method with respect to the sample window. Algorithm behavior in the presence of events that may often occur in power systems, such as voltage dips and swells, can be inferred from amplitude step results, assuming they can be seen as a close succession of step variations.

Finally, it may also be of interest to consider the case of a frequency step. The plot of Fig. 5 shows the TVE during a 1-Hz step (as in [12]), e.g. from 50 Hz to 49 Hz, when an interharmonic at 76 Hz is also present as in previous tests. Response time is even shorter (about 20 ms) than for the amplitude step. The frequency estimate transitions smoothly between the two values.

V. Conclusion

In this paper a novel approach for synchrophasor estimation, based on compressive sensing super-resolution for a Taylor-Fourier multifrequency model (CSTFM) has been introduced. Its performance has been characterized under different static and dynamic conditions, using composite test signals that include various disturbances, such as interharmonics, harmonics and additive noise, in an attempt to represent a severe operating environment.

CSTFM allows to detect with a good resolution the relevant spectral components of the signal, even when they are changing with time, while keeping the observation interval reasonably low. The algorithm is promising in its ability to cope with severe operating conditions, like the concurrent effect of dynamic conditions and interharmonic interference, with remarkable performance in terms of estimation accuracy.

References

[1] *IEEE Standard for Synchrophasor Measurements for Power Systems*, IEEE Std C37.118.1-2011 (Revision of IEEE Std C37.118-2005), Dec. 2011.

[2] *IEEE Standard for Synchrophasor Measurements for Power Systems – Amendment 1: Modification of Selected Performance Requirements*, IEEE Std C37.118.1a-2014 (Amendment to IEEE Std C37.118.1-2011), Apr. 2014.

[3] J. A. de la O Serna, "Dynamic phasor estimates for power system oscillations," *IEEE Trans. Instrum. Meas.*, vol. 56, no. 5, pp. 1648–1657, Oct. 2007.

[4] W. Premerlani, B. Kasztenny, and M. Adamiak, "Development and implementation of a synchrophasor estimator capable of measurements under dynamic conditions," *IEEE Trans. Power Del.*, vol. 23, no. 1, pp. 109–123, Jan. 2008.

[5] R. K. Mai, Z. Y. He, L. Fu, B. Kirby, and Z. Q. Bo, "A dynamic synchrophasor estimation algorithm for online application," *IEEE Trans. Power Del.*, vol. 25, no. 2, pp. 570–578, Apr. 2010.

[6] M. A. Platas-Garza and J. A. de la O Serna, "Dynamic phasor and frequency estimates through maximally flat differentiators," *IEEE Trans. Instrum. Meas.*, vol. 59, no. 7, pp. 1803–1811, Jul. 2010.

[7] M. Karimi-Ghartemani, B.-T. Ooi, and A. Bakhshai, "Application of enhanced phase-locked loop system to the computation of synchrophasors," *IEEE Trans. Power Del.*, vol. 26, no. 1, pp. 22–32, Jan. 2011.

[8] M. A. Platas-Garza and J. A. de la O Serna, "Dynamic harmonic analysis through Taylor-Fourier transform," *IEEE Trans. Instrum. Meas.*, vol. 60, no. 3, pp. 804–813, Mar. 2011.

[9] J. Liu, F. Ni, P. A. Pegoraro, F. Ponci, A. Monti, and C. Muscas, "Fundamental and harmonic synchrophasors estimation using modified Taylor-Kalman filter," in *Applied Measurements for Power Systems (AMPS), 2012 IEEE International Workshop on*, Sep. 2012, pp. 1–6.

[10] D. Belega and D. Petri, "Accuracy analysis of the multicycle synchrophasor estimator provided by the interpolated DFT algorithm," *IEEE Trans. Instrum. Meas.*, vol. 62, no. 5, pp. 942–953, May 2013.

[11] A. J. Roscoe, I. Abdulhadi, and G. Burt, "P and M class phasor measurement unit algorithms using adaptive cascaded filters," *IEEE Trans. Power Del.*, vol. 28, no. 3, pp. 1447–1459, Jul. 2013.

[12] C. Orallo, I. Carugati, S. Maestri, P. Donato, D. Carrica, and M. Benedetti, "Harmonics measurement with a modulated sliding discrete Fourier transform algorithm," *IEEE Trans. Instrum. Meas.*, vol. 63, no. 4, pp. 781–793, Apr. 2014.

[13] D. Belega and D. Petri, "A real-valued Taylor weighted least squares synchrophasor estimator," in *Applied Measurements for Power Systems Proceedings (AMPS), 2014 IEEE International Workshop on*, Sep. 2014, pp. 1–6.

[14] D. Petri, D. Fontanelli, and D. Macii, "A frequency-domain algorithm for dynamic synchrophasor and frequency estimation," *IEEE Trans. Instrum. Meas.*, vol. 63, no. 10, pp. 2330–2340, Oct. 2014.

[15] M. Bertocco, G. Frigo, C. Narduzzi, and F. Tramarin, "Resolution enhancement by compressive sensing in power quality and phasor measurement," *IEEE Trans. Instrum. Meas.*, vol. 63, no. 10, pp. 2358–2367, Oct. 2014.

[16] P. Romano and M. Paolone, "Enhanced interpolated-DFT for synchrophasor estimation in FPGAs: Theory, implementation, and validation of a PMU prototype," *IEEE Trans. Instrum. Meas.*, vol. 63, no. 12, pp. 2824–2836, Dec. 2014.

[17] P. Castello, M. Lixia, C. Muscas, and P. A. Pegoraro, "Impact of the model on the accuracy of synchrophasor measurement," *IEEE Trans. Instrum. Meas.*, vol. 61, no. 8, pp. 2179–2088, Aug. 2012.

[18] G. Barchi, D. Macii, and D. Petri, "Synchrophasor estimators accuracy: A comparative analysis," *IEEE Trans. Instrum. Meas.*, vol. 62, no. 5, pp. 963–973, May 2013.

[19] G. Barchi, D. Macii, D. Belega, and D. Petri, "Performance of synchrophasor estimators in transient conditions: A comparative analysis," *IEEE Trans. Instrum. Meas.*, vol. 62, no. 9, pp. 2410–2418, Sept 2013.

[20] D. Belega, D. Macii, and D. Petri, "Fast synchrophasor estimation by means of frequency-domain and time-domain algorithms," *IEEE Trans. Instrum. Meas.*, vol. 63, no. 2, pp. 388–401, Feb. 2014.

[21] P. Castello, M. Lixia, C. Muscas, and P. A. Pegoraro, "Adaptive Taylor-Fourier synchrophasor estimation for fast response to changing conditions," in *Instrumentation and Measurement Technology Conference (I2MTC), 2012 IEEE International*, May 2012, pp. 294–299.

[22] P. Castello, P. Ferrari, A. Flammini, C. Muscas, and S. Rinaldi, "A new IED with PMU functionalities for electrical substations," *IEEE Trans. Instrum. Meas.*, vol. 62, no. 12, pp. 3209–3217, Dec. 2013.

[23] A. Roscoe, "Exploring the relative performance of frequency-tracking and fixed-filter phasor measurement unit algorithms under c37.118 test procedures, the effects of interharmonics, and initial attempts at merging P-class response with M-class filtering," *Instrumentation and Measurement, IEEE Transactions on*, vol. 62, no. 8, pp. 2140–2153, Aug. 2013.

[24] P. Castello, J. Liu, A. Monti, C. Muscas, P. A. Pegoraro, and F. Ponci, "Toward a class "P + M" phasor measurement unit," in *Applied Measurements for Power Systems (AMPS), 2013 IEEE International Workshop on*, Sep. 2013, pp. 91–96.

[25] P. Castello, J. Liu, C. Muscas, P. A. Pegoraro, F. Ponci, and A. Monti, "A fast and accurate PMU algorithm for P+M class measurement of synchrophasor and frequency," *IEEE Trans. Instrum. Meas.*, vol. 63, no. 12, pp. 2837–2845, Dec. 2014.

[26] M. Platas-Garza and J. de la O Serna, "Polynomial implementation of the Taylor-Fourier transform for harmonic analysis," *IEEE Trans. Instrum. Meas.*, vol. 63, no. 12, pp. 2846–2854, Dec. 2014.

[27] M. Chakir, I. Kamwa, and H. Le Huy, "Extended C37.118.1 PMU algorithms for joint tracking of fundamental and harmonic phasors in stressed power systems and microgrids," *IEEE Trans. Power Del.*, vol. 29, no. 3, pp. 1465–1480, Jun. 2014.

[28] J. de la O Serna, "Synchrophasor measurement with polynomial phase-locked-loop Taylor-Fourier filters," *IEEE Trans. Instrum. Meas.*, vol. 64, no. 2, pp. 328–337, Feb. 2015.

[29] M. Bertocco, G. Frigo, and C. Narduzzi, "On compressed sensing and super-resolution in dft-based spectral analysis," in *Proceedings 19th IMEKO TC-4 Symposium and 17th IWADC Workshop Advances in Instrumentation and Sensors Interoperability*, Jul 2013, pp. 615–620.

[30] G. Frigo and C. Narduzzi, "Compressive sensing with an overcomplete dictionary for high-resolution dft analysis," in *Signal Processing Conference (EUSIPCO), 2014 Proceedings of the 22nd European*, Sept 2014, pp. 1766–1770.

[31] M. Bertocco, G. Frigo, C. Narduzzi, C. Muscas, and P. A. Pegoraro, "Compressive sensing plus Taylor-Fourier Transform for synchrophasor estimation," in *Applied Measurements for Power Systems Proceedings (AMPS), 2014 IEEE International Workshop on*, Sep. 2014, pp. 1–5.

[32] C. Qian, T. Bi, J. Li, H. Liu, and Z. Liu, "Synchrophasor estimation algorithm using legendre polynomials," in *PES General Meeting — Conference Exposition, 2014 IEEE*, Jul. 2014, pp. 1–5.

[33] J. Tropp and A. Gilbert, "Signal recovery from random measurements via orthogonal matching pursuit," *Information Theory, IEEE Transactions on*, vol. 53, no. 12, pp. 4655–4666, Dec 2007.

[34] *IEEE Guide for Synchronization, Calibration, Testing, and Installation of Phasor Measurement Units (PMUs) for Power System Protection and Control*, IEEE Std C37.242-2013, Mar. 2013.

Matteo Bertocco received the Laurea degree in electronics engineering from the University of Padova, where he subsequently received the Ph.D degree in electronics engineering in 1991. Since 1994, he has worked as a Researcher at the Department of Electronics and Informatics, University of Padova, becoming an Associate Professor of Electronic Instrumentation and Measurement in 1998, and full professor in 2002. He is director of the PhD school in Information Engineering. His research interests are in wireless sensor networks, automated instrumentation and electromagnetic compatibility. He is author of over 130 technical papers published on international Journals and Conference Proceedings. He is research associate member of CNR-IEEIT since 2011, and member of the IEEE since 1987.

Guglielmo Frigo was born in Padova in 1986. He received the B.Sc. and M.Sc. degrees in Biomedical Engineering from the University of Padova in 2008 and 2011, respectively. In 2015 he earned a Ph.D. degree at the School of Information Engineering in the University of Padova with a dissertation about Compressive Sensing (CS) theory applications to instrumentation and measurement scenario. He joined the Electronic Measurement research group in 2011 and collaborated in the successful development of CS-based algorithms in the fields of spectral analysis, biomedical engineering and smart-grid measurement and is the coauthor of several conference and journal papers on these topics.

Claudio Narduzzi was born in Venice, Italy, in 1958. He received the Laurea degree (cum laude) in Electronics engineering from the University of Padova in 1982. He is a full Professor in Instrumentation and Measurement at the Engineering School of the University of Padua, where he has been Director of Taught Programmes in Electronics Engineering between 2008 and 2012. He has worked on several instrumentation-related topics in the areas of electronics and telecommunications, including spectral analysis, inverse filtering, circuit testing, quantization and analogue-to-digital conversion. His current research interests are networked measuring systems, digital signal processing applications in measurement, instrumentation and test system characterization. Prof. Narduzzi is the author of over 150 scientific papers and of textbooks for academic courses. He is a member of IEEE.

Carlo Muscas (M'98) received the M.S. (cum laude) degree in electrical engineering from the University of Cagliari, Cagliari, Italy, in 1994.

He was Assistant Professor with the University of Cagliari from 1996 to 2001. He has been an Associate Professor of Electrical and Electronic Measurement with the University of Cagliari, since 2001, where he is currently the Chairman of the Council for the M. S. degree in Electrical Engineering. He has authored or co-authored over 120 scientific papers. His current research interests include power quality phenomena, the measurement of synchronized phasors and the implementation of distributed measurement systems for modern electric grid.

Mr. Muscas is currently an Associate Editor of the IEEE Transactions on Instrumentation and Measurement.

Paolo Attilio Pegoraro (S'03-M'06) received the M.S. (cum laude) degree in telecommunications engineering and the Ph.D. degree in electronic and telecommunications engineering from the University of Padua, Padua, Italy, in 2001 and 2005, respectively.

He currently holds a post-doctoral position with the University of Cagliari, Cagliari, Italy, where he focuses on the development of new measurement techniques for modern power networks. His current research interests include the measurement of synchronized phasors and the state estimation for electric distribution grids.